Large-Scale 3D-Printable Bending-Active Formwork with Auxetic Properties

Kazunori Nakayama[1], Hiroki Awaji[2], Yusuke Sakai[3], Ryo Yoshikawa[4], Sei Hayashi[5], Tomoyuki Gondo[6], Toshiaki Kimura[7] and Eisuke Mitsuda[8]
[1,6]*The University of Tokyo*
[2]*Asahi Building-Wall CO., LTD.*
[3]*Sony Computer Science Laboratories - Kyoto*
[4,7]*Nagoya City University*
[5]*Tokyo Metropolitan University*
[8]*Kyoto Institute of Technology*
[1]*kazu@g.ecc.u-tokyo.ac.jp, 0009-0000-3943-1703*
[2]*hiroki-awaji@agb.co.jp, 0000-0003-2639-0556*
[3]*Yusuke. C.Sakai@sony.com, 0000-0003-3660-4247*
[4]*c255727@ed.nagoya-cu.ac.jp, 0009-0008-6134-7485*
[5]*hayashisei@tmu.ac.jp, 0000-0003-1874-4991*
[6]*gondo@arch1.t.u-tokyo.ac.jp, 0000-0002-6125-865X*
[7]*tkimura@sda.nagoya-cu.ac.jp, 0000-0001-8570-1073*
[8]*mitsuda@kit.ac.jp, 0009-0007-0636-5835*

Abstract. This study presents an enhanced method for fabricating large-scale bending-active formwork with auxetic properties using pellet-based three-dimensional (3D) printing. Previous work demonstrated the feasibility of constructing auxetic bending-active grid shells using filament-based printing; however, the small printable blocks of approximately 300 mm × 300 mm significantly increased fabrication time and assembly effort. Here, a scalable workflow capable of producing 1 m × 1 m blocks is developed to reduce fabrication time while maintaining structural performance. A continuous single-path printing strategy is adopted to enable rapid block production. In addition, a toolpath design that follows different routes every four layers is implemented to enhance overall stability. Because pellet-based extrusion produces rounded edges that complicate alignment, three joining techniques, namely welding, fusion welding and hot-melt adhesive, are examined. Among these, fusion welding achieves stable bonding under deformation. The methodology integrates computational grid design, material selection, process parameter control and structural evaluation through load–displacement testing. The results show that the proposed system substantially reduces printing time while achieving mechanical behaviour comparable to that of the filament-based approach. Pellet-based 3D printing therefore represents a viable approach for fabricating large-scale bending-active formworks.

HUMANISTIC COMPUTATION AND INTELLIGENCE, Proceedings of the 31st International Conference of the Association for Computer-Aided Architectural Design Research in Asia (CAADRIA) 2026, Volume 2, 503-512.

Keywords. Auxetic Structure, 3D-Printed Formwork, Free-Form Shell, Non-Developable Surface, Reusable Materials

1. Introduction

Recent advances in digital design tools, such as three-dimensional (3D) computer-aided design and building information modelling, have enabled architectural design with complex free-form surfaces. However, non-developable free-form surfaces present numerous construction challenges, including difficulties in transporting large 3D components and limitations on material reusability due to geometric complexity. Consequently, extensive research has focused on construction strategies that apply computational form-finding and digital fabrication techniques (Scheder-Bieschin et al., 2024; Kimura et al., 2024).

Form-finding strategies for bending-active grid shells have been widely investigated (Lienhard et al., 2013). Bending-active grid shells can support the development of efficient formwork systems because structural forms can be constructed with fewer auxiliary supports. Auxetics are materials or structures characterised by a negative Poisson's ratio, and the application of auxetic structures has also been extensively studied (Isvoranu et al., 2021). Owing to their auxetic behaviour, auxetic bending-active grid shells (ABAG) can be deformed from an initial flat grid with boundary supports into a dome-like surface with positive Gaussian curvature (Sakai et al., 2021). By combining auxetic and non-auxetic patterns within the initial flat grid, the proposed formwork can also be deformed into complex curved surfaces with both positive and negative Gaussian curvatures. To achieve the desired shape, the grid pattern of the initial flat grid is computationally designed through large-deformation analysis.

In our previous study, a prototype glass fibre-reinforced concrete shell measuring 4.0 m in width, 2.7 m in depth and 1.4 m in height was constructed using ABAG as formwork (Figure 1). Filament-based 3D printing was employed to fabricate structural blocks forming the initial flat grid of the ABAG. Thermoplastic polyurethane (TPU), a flexible material, was used to ensure sufficient deformability of the printed blocks. An ABAG surface with high geometric precision was successfully constructed. However, filament-based 3D printing required substantial printing time because of the narrow nozzle diameter. In addition, the limited printable size of individual components resulted in significant fabrication effort, as numerous small blocks had to be manually connected by welding to form a large-scale initial flat grid.

To address these limitations, this study employs pellet-based 3D printing as an enhanced fabrication approach for large-scale bending-active formwork systems. The scalability of the system for architectural applications is examined through the fabrication and performance evaluation of a 3 m × 3 m mock-up model. Pellet-based 3D printers provide access to industrial-grade TPU materials with improved mechanical and thermal properties compared with previously used general-purpose filaments. First, optimal pellet extrusion parameters for fabricating a large-scale initial flat grid are investigated. TPU grade selection and associated printer settings, including temperature control and extrusion rates, are evaluated.

Second, the toolpath design methodology for the initial flat grid blocks is updated

to accommodate the constraints of pellet-based 3D printing. In previous work, the grid was fabricated following its exact geometry; however, with pellet-based printers, the large nozzle diameter and the difficulty of stopping material extrusion during printing make it challenging to achieve the intended geometry unless the block shape is designed as a continuous single path. Printing time using pellet-based 3D printing is then evaluated and compared with that of filament-based printing used in the previous study. The mechanical behaviour of the initial flat grid composed of the updated blocks is also investigated. These preliminary tests demonstrate the feasibility of fabricating the proposed formwork system using pellet-based 3D printing and indicate substantial reductions in both printing time and the number of required joints compared with filament-based fabrication. Finally, a 3 m × 3 m mock-up model is developed using the updated design methodology, and its effectiveness is evaluated through a comparative assessment of printing time, welding labour and structural performance.

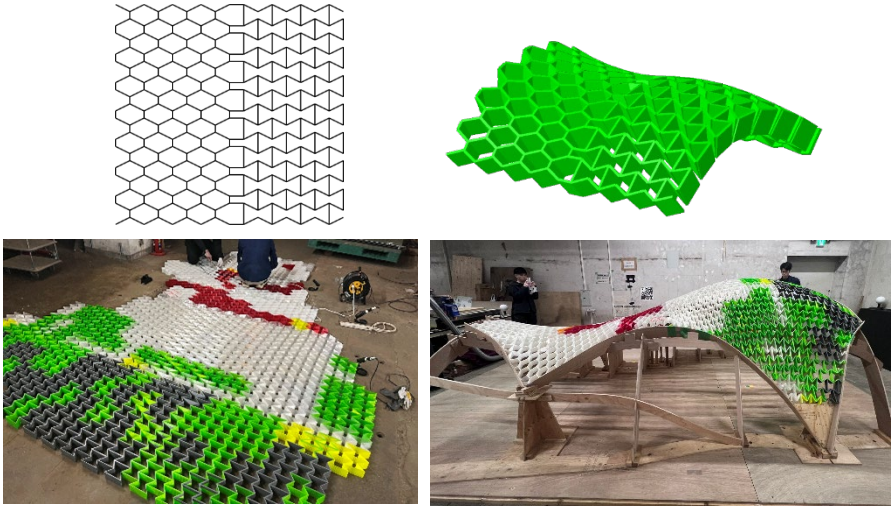

Figure 1. Composition of ABAG with hexagonal units (top left) and deformation (top right), initial flat grid of the ABAG mock-up (bottom left), and ABAG curved surface (bottom right)

2. Pellet-based 3D Printing and Toolpath Design

In this study, the GEM1000S (S. lab) is used to fabricate the ABAG. The system can produce 3D-printed objects up to 1.0 m × 1.2 m × 1.0 m using various grades of TPU.

First, a feasibility study of TPU 3D printing is conducted to determine optimal printing parameters, including nozzle diameter, nozzle temperature, ejecting rate (extruded pellet weight per second), nozzle velocity and first-layer height for producing appropriate TPU components. Based on this study, the nozzle temperatures are set to 160°C, 175°C, 180°C and 185°C across four heating zones from top to bottom, respectively. The remaining parameters are determined as summarised in Table 1.

Unlike filament-based 3D printing, which allows frequent retraction, pellet-based extrusion relies on a constant material flow and must be executed as a single continuous stroke. This requirement necessitates a graph-theoretical reconstruction of the toolpath,

as illustrated in Figure 2:

- Step 1: Connecting multiple units creates numerous nodes at which three members meet. An Eulerian path, which enables a single continuous stroke, is only possible when the number of odd-degree nodes is zero or two.
- Step 2: Specific edges are duplicated to convert internal nodes into even-degree nodes. This process establishes a topologically continuous path in which only the start and end points remain odd-degree nodes.
- Step 3: To prevent over-extrusion at intersections, junctions are split into two filleted curves. The offset distance is determined based on the printing bead width.
- Step 4: The final output is a seamless, continuous toolpath that ensures stable extrusion throughout the process and prevents fabrication defects.

Table 1. 3D-printing parameters

Nozzle diameter (mm)	Ejecting rate (g/s)	Nozzle velocity (mm/s)	First layer height (mm)
4	1.5	30	2
5	1.5	40	2.5
10	1.3	30	5

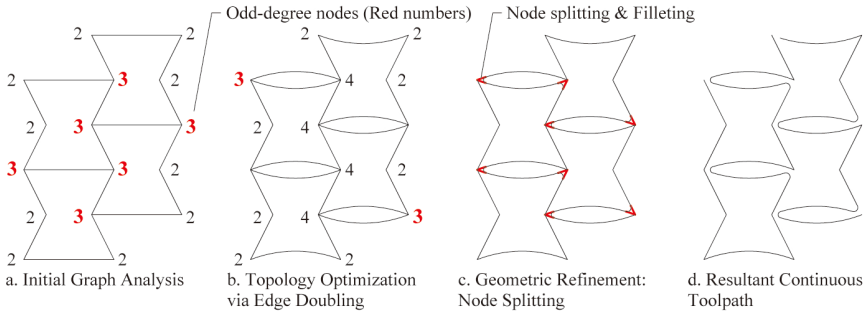

Figure 2. Reconstructed toolpath for hexagonal units with auxetic properties

In general pellet-based 3D-printing processes, overlapping passes at corners can compromise build accuracy because of excessive material accumulation in the vertical direction. To address this issue, toolpaths at corners are assigned an offset that allows an overlap of only 1/20 of the ABAG member width, as shown on the left side of Figure 3. In addition, layers are repeatedly stacked using four distinct toolpaths as units, as shown on the right side of Figure 3, to enhance overall stability.

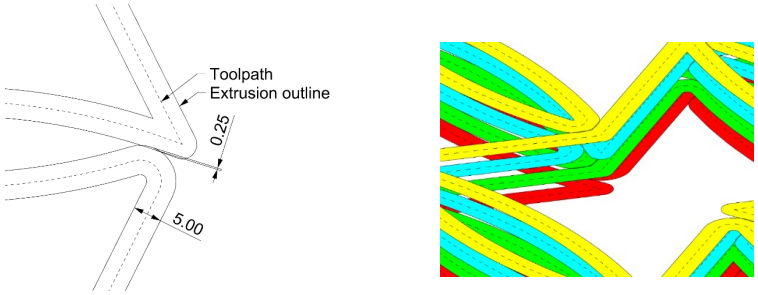

Figure 3. Enlarged view of the corner of the reconstructed hexagonal unit (left) and stacked layers using four distinct toolpaths (right) (unit: mm)

3. Comparison with Filament-based 3D printing

3.1. PRINTING TIME

Printing time was compared using a block extracted from the initial flat grid shown in Figure 4. The BigRep BLADE was used to estimate the printing time for filament-based 3D printing. The cross-sectional dimensions of the block members were examined for two cases: 5 mm × 50 mm and 10 mm × 100 mm. Table 2 summarises the results for both printing methods. As shown in Table 2, pellet-based 3D printing substantially reduces printing time compared with filament-based 3D printing. Notably, the pellet-based 3D printer maintains an almost constant printing time despite an increase in cross-sectional area.

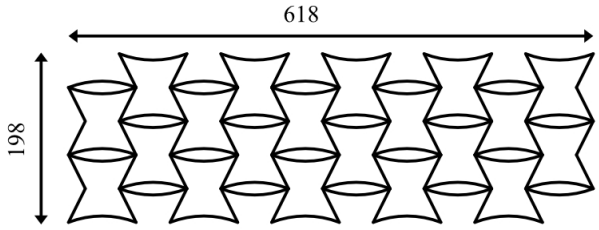

Figure 4. Dimensions of the experimental model for estimating printing time (unit: mm)

Table 2. Printing time

Nozzle diameter (mm)	3D printer	Cross section (mm)	Printing time
5	GEM1000S	5×50	1 hrs. 23 min. 39 sec.
10		10×100	1 hrs. 49 min. 58 sec.
0.6	Big Rep	5×50	70 hrs. 9 min.
		10×100	94 hrs. 13 min.

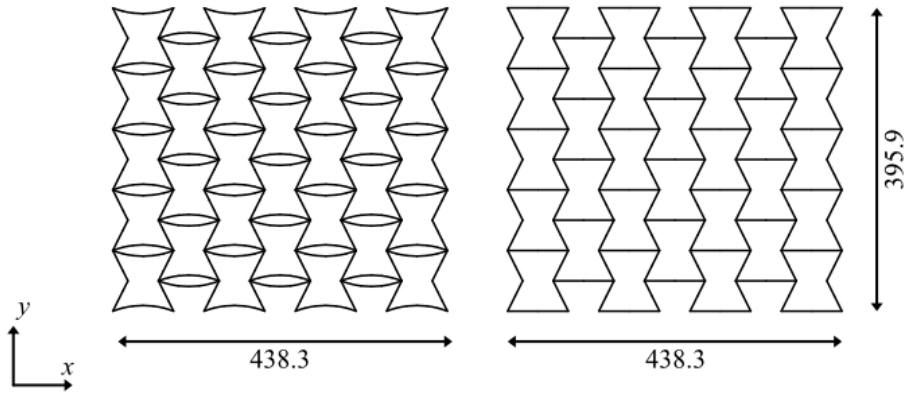

Figure 5. Block composed of reconstructed hexagonal units (left: Model A) and the original block from a previous study (right: Model B) (unit: mm)

3.2. STRUCTURAL INVESTIGATION

The block composed of reconstructed hexagonal units described in Section 2 (Model A) is compared with a block composed of the original units from a previous study (Model B). In both models, 35 units (7 × 5) with identical dimensions are arranged within blocks measuring 438.3 mm × 395.9 mm, as shown in Figure 5. Post-buckling analyses were conducted using Abaqus to compare the structural performance of the two blocks. The initial flat grids were modelled as beam elements with a rectangular cross section of 5 mm × 50 mm. The material was defined as TPU with a Young's modulus of 40 GPa, a Poisson's ratio of 0.49 and a density of 1.14 t/m^3. Figure 6 illustrates the boundary conditions and load directions applied to Model A. Multi-point constraints were assigned along the left and right edges. Pin-supported reference nodes constrained the slave nodes. A geometric imperfection was introduced using the first Eigen buckling mode with an amplitude of 1 mm. Forced displacements were applied to the reference nodes along the x- or y-axis. The black arrows indicate the directions of the forced displacements applied at the two supporting points. Four numerical cases were examined. The case in which Model A was subjected to forced displacement in the x-direction is referred to as Case Ax. The remaining cases are denoted Case Ay, Case Bx and Case By in the same manner.

Figure 7 presents the load–displacement curves of the two blocks. The red and orange curves correspond to Cases Ax and Ay, respectively, while the blue and green curves represent the results of Cases Bx and By. As shown in Figure 7, the mechanical behaviours of the two blocks, including elastic stiffness and buckling strength, are nearly equivalent despite the geometric differences between them. This result indicates that shape variations introduced by the toolpath design in 3D printing do not significantly affect the mechanical behaviour.

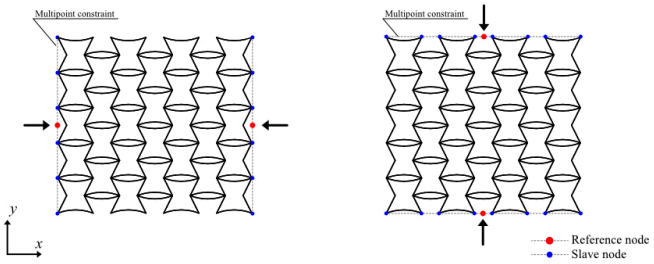

Figure 6. Boundary conditions and load directions in Model A

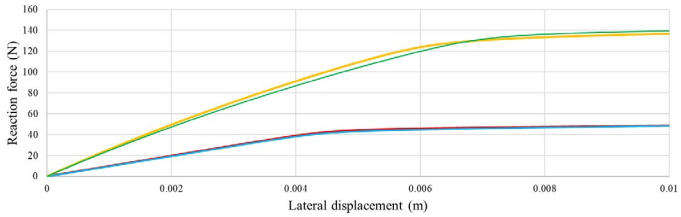

Figure 7. Load–displacement curves of the two blocks (red: Case Ax, orange: Case Ay, blue: Case Bx, green: Case By)

4. Mock-up Model

4.1. DIMENSIONS

The curved surface of the mock-up model is constructed by actively bending an initial flat grid with rectangular dimensions of 2.7 m × 3.3 m, as shown in Figure 8. The initial flat grid consists of two types of blocks measuring 0.9 m × 1.1 m, which are discretised into beam elements with a rectangular cross section of 5 mm × 50 mm. The material is TPU, as defined in Section 3.2. During the active bending process, the upper and lower edges of each initial flat grid, as illustrated in Figure 8, are simply supported. Karamba3D, a finite element analysis software for Rhinoceros and Grasshopper, is used to obtain the curved shapes. As shown in Figure 9, two types of curved surfaces are generated by rearranging the blocks of the initial flat grids. The effectiveness of pellet-based 3D printing is validated through the reconfiguration of the pellet-based 3D-printed blocks.

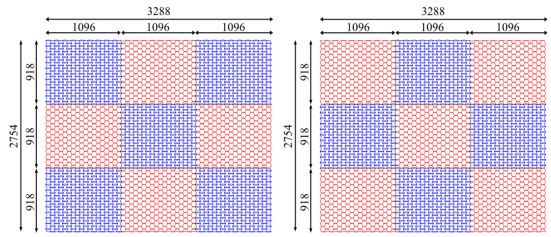

Figure 8. Initial flat grid for the mock-up model (unit: mm) (left: pattern 1, right: pattern 2)

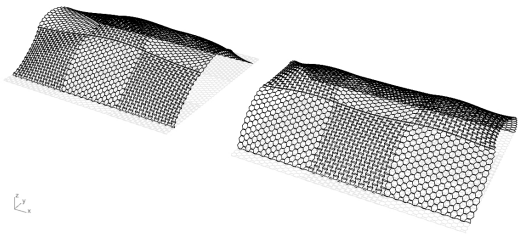

Figure 9. Obtained curved surfaces (left: pattern 1, right: pattern 2)

4.2. 3D PRINTING

The blue-coloured auxetic pattern of the initial flat grid for the mock-up model, shown in Figure 9, was experimentally fabricated using pellet-based 3D printing. Figure 10 shows the printed block. The printing time for a single block was 10.02 h.

Figure 10. 3D-printed block (unit: mm)

In previous research, the 3D printers Prusa MK3, MK4, Bambulab A1 and H2D were used to fabricate an initial flat grid with a total area of 9.0 m². Owing to build size limitations, 321 blocks were required. The 3D-printing process took 41 days (January to February 2025) using 11 printers (Prusa: 7 units; Bambulab: 4 units). Accordingly, the printable area per day can be calculated as 9.0/41 = 0.22 m²/day. Using the same approach, the printable area achieved with the pellet-based 3D printer in this study is estimated as 1.0/(10.02/24) = 2.39 m²/day. These results demonstrate that pellet-based 3D printing substantially reduces printing time compared with filament-based fabrication.

4.3. JOINT

A suitable joint method must be considered to realise the mock-up model composed of 3D-printed elements. Objects fabricated using filament-based 3D printing can be joined relatively easily owing to the ability to produce precise geometries. In contrast, joining objects fabricated using pellet-based 3D printing presents challenges because of rounded edges and reduced contact areas. In this study, suitable bonding methods for pellet-printed units were investigated through strength tests using three techniques: welding, in which a filament is melted along a groove to form a continuous seam; fusion welding; and hot-melt adhesive.

The printing parameters were identical to those used for fabricating the mock-up model. Test specimens were prepared by joining printed elements with dimensions of 80 mm in width, 280 mm in depth and 50 mm in height using the different joint configurations. Flexural performance was evaluated through three-point bending tests conducted using a Tensilon RTF-1350 universal testing machine. The span length was set to 110 mm, and the load was applied at the mid-span. The loading rate was 10 mm/min, and one specimen was tested for each condition ($N = 1$).

Figure 11 shows the load–displacement curves, elastic stiffness K (N/mm) and maximum load P (N) for specimens prepared using each joining method, allowing a comparison of their structural performance. Welding exhibited the highest stiffness; however, the load-bearing capacity dropped abruptly after reaching the maximum load. Fusion welding demonstrated slightly lower stiffness than welding, but the load decreased gradually after the peak, indicating higher durability. The hot-melt adhesive showed the lowest stiffness and exhibited inferior durability. From a workability perspective, welding required inserting the soldering iron deeply into relatively large gaps. Because of this requirement, variations in gap width sometimes prevented the formation of a complete joint. The hot-melt adhesive was easier to apply, and deeper injection is expected to improve its strength. Fusion welding produced the most reliable joints because the gap width closely matched the filament diameter, allowing uniform filling.

For this application, it is essential that the joint prevents brittle collapse. Considering its high durability and sufficient workability, fusion welding demonstrated the highest overall performance and was therefore adopted for the mock-up model.

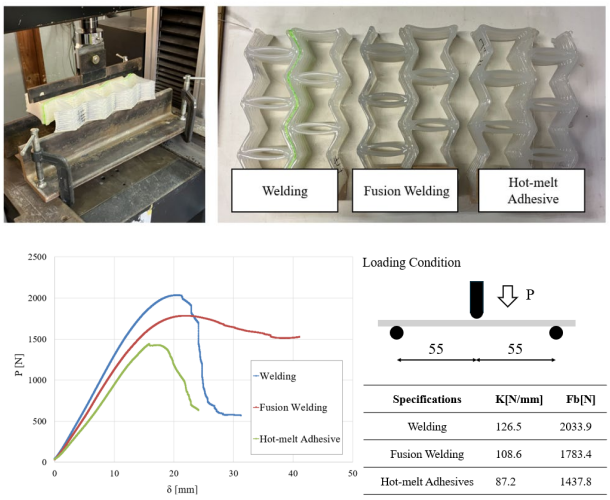

Specifications	K[N/mm]	Fb[N]
Welding	126.5	2033.9
Fusion Welding	108.6	1783.4
Hot-melt Adhesives	87.2	1437.8

Figure 11. Comparison of bending strength and stiffness

5. Discussion and Conclusion

This study proposes a bending-active formwork system fabricated using pellet-based 3D printing. To enable pellet-based fabrication, a continuous single-path printing

methodology was introduced, allowing the production of blocks without interruptions in material extrusion. In addition, a toolpath generation method that follows different routes every four layers was developed to enhance overall structural stability. Physical experiments indicated that the use of pellet-based 3D printing reduced fabrication time by more than 90%. Although pellet-based 3D printing results in rounded edge profiles that complicate precise alignment, several joining techniques, including welding, fusion welding and hot-melt adhesive, were examined. Among these, fusion welding provided the most favourable performance for unit-to-unit connections.

The flexibility of 3D printing, which is a key feature of this study, enables versatile curvature control through adaptable member placement. The realisation of large-scale blocks represents a transition of the proposed method from an experimental stage toward practical architectural production. Furthermore, post-buckling analyses demonstrated that the proposed fabrication method achieves structural performance comparable to that of the previous filament-based approach. The fabrication of blocks for the mock-up model further confirmed both the substantial reduction in printing time and the adequate quality of the ABAG elements. Overall, these findings verify the feasibility of employing pellet-based 3D printing for the efficient production of large-scale bending-active formwork. Future research will focus on developing fixation mechanisms for shape retention and exploring geometric reconfiguration through the reuse of printed blocks.

Acknowledgements

This work was supported by JST SPRING, Grant Number JPMJSP2108 and JSPS KAKENHI (Grants-in-Aid for Scientific Research) No. 24K01031; and Mr Tomohiro Inoue (KYOTO Design Lab) for technical assistance.

References

Isvoranu, F., Chen, T., Bouleau, E., Blanc, A., Dietz, D., et al. (2021). The Canopy Pavilion: A lightweight shading structure using a deployable auxetic linkage membrane. In Advances in Architectural Geometry 2020 (AAG 2020) (pp. 376–390). Online Conference, April 26–29. http://infoscience.epfl.ch/record/297530

Kimura, T., Hayashi, S., Muto, T., Yamasaki, K., Sakai, Y., & Gondo, T. (2024). Form-finding for free-curved reinforced concrete shell structure considering structural performance and construction formwork. Engineering Structures, 301, 117332. https://doi.org/10.1016/j.engstruct.2023.117332

Lienhard, J., Alpermann, H., Gengnagel, C., & Knippers, J. (2013). Active bending: A review of structures where bending is used as a self-formation process. International Journal of Space Structures, 28(3–4), 187–196. https://doi.org/10.1260/0266-3511.28.3-4.187

Sakai, Y., & Ohsaki, M. (2021). Optimization method for shape design of Auxetic Bending-Active Gridshells using discrete differential geometry. Structures, 34, 1589–1602. https://doi.org/10.1016/j.istruc.2021.08.067

Scheder-Bieschin, L., Van Mele, T., & Block, P. (2024). Bending-active formwork systems for concrete shells – a classification and state-of-the-art review. Structures, 67, 106841. https://doi.org/10.1016/j.istruc.2024.106841